Effect of the undulator in IR4 on the LHC beam

François Méot[*] and André Verdier

December 7, 2013

Abstract

An undulator is installed in IR4 to produce synchrotron radiation. The perturbation it introduces in LHC is examined. It has little effect on the closed orbit, a negligible effect on the tune. Its intrinsic non-linearities are negligible (analysis by ray tracing). Specifications on the multipole content of its integrated field are given to produce no effect on the dynamic aperture.
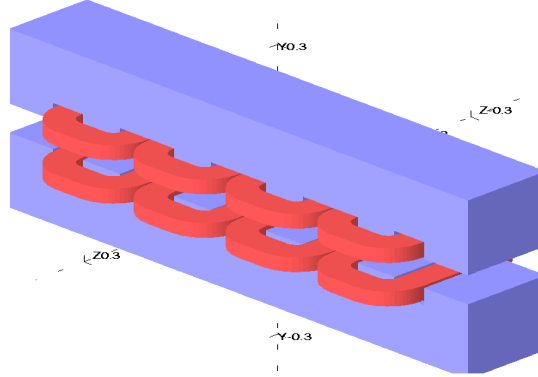
---
[*]CEA DAPNIA, Saclay

Figure 1: Schematic view of the undulator

1 Introduction

The determination of the beam size in LHC can be done with several devices [1]. One of them is based on the detection of the synchrotron radiation emitted by a special undulator [2] consisting of four alternating magnetic poles (see fig. 1) housed in IR4 as shown on figure 2.

The integral of the magnetic field on the axis is zero. The field description is examined in section 2. A beam passing though this device does not get any deflection but a displacement perpendicular to the entrance trajectory. The associated closed orbit distortion is evaluated in Section 3. The effect on the tunes is evaluated in Section 4.

It is worth evaluating the importance of this wiggler with simple comparisons. In synchrotron light machines, wigglers are introduced which perturb significantly the linear optics (see for instance [3] in which the lattice encompasses matching quadrupoles to accommodate the wiggler). It is straightforward to test the importance of such a perturbation with a simple model with hard edge dipoles. It appears that the LHC wiggler is less important than that described in [3] by about four orders of magnitude, which is confirmed by the simple model. The non-linear effect are also reduced accordingly, they are associated with the longitudinal variation of the field and are examined in Sections 5. Conventional 2D specifications on multipole components are relevant and are given in Section 6.

2 Description of the undulator field.

The variation of the vertical magnetic field on the axis of the undulator is shown in Figure 3. The integrated magnetic field is zero on the axis.

For ray tracing the model of the field on the axis as given on figure 3, together with the assumption of invariance by x-translation (transverse to the beam), is sufficient to compute the value of the field off-axis by expanding it in Taylor series and putting them in Maxwell equations.

For the MADX computation, the undulator effect can be modeled by describing the undulator with a sequence of dipoles. Actually a sequence of closed orbit correctors is
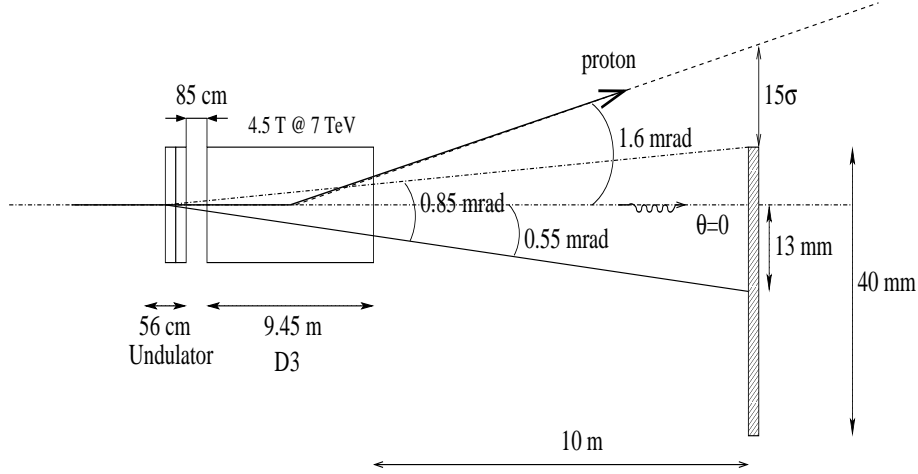
Figure 2: Installation of the undulator close to the dipole D3 in IR4. The synchrotron radiation is observed on a screen 10m from D3 while the proton beam is deflected by D3.

used.

The simplest model consists of four dipoles of length $l = 0.14$m. Each dipole has a constant magnetic field B given by $B = 2\hat{B}/\pi$, so that the integrated field of each piece is equal to that of half an oscillation of the field shown on Figure 3 (note that the small oscillations at both ends have been neglected). This model has the advantage of a simple analytic treatment.

A more accurate model has been constructed to reproduce the angles and displacement obtained by ray tracing. Each undulation of the field is described by a sequence of six dipoles of length ld=0.02m with fields equal respectively to $\hat{B}\sin(\pi$ dl / 0.14), $\hat{B}\sin(2\pi$ dl / 0.14) and $\hat{B}\sin(3\pi$ dl / 0.14). With this model it is possible to reproduce the trajectory shown on figure 4.

3 Effect of the dipole component.

Although the undulator gives no kick, it produces a transverse displacement of the particle trajectories. The integration of the trajectories (ray tracing) by means of the code ZGOUBI [4] produces a displacement shown on figure 4. The overall displacement is 35μm.

The four dipole model overestimates the displacement which is four times the displacement due to a single dipole, i.e. 65μm (the field overshoot at the end has been neglected).

The maximum closed orbit distortion obtained by ray tracing is 30μm. The maxi-
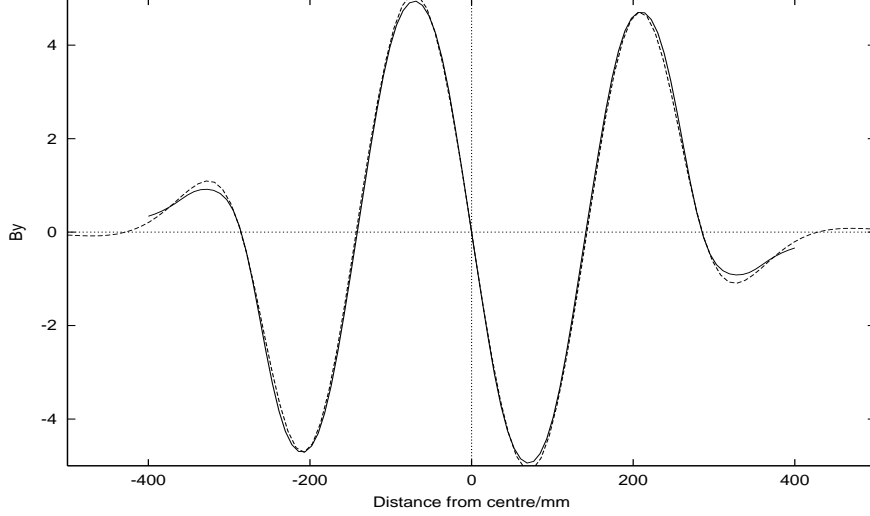
Figure 3: Longitudinal variation of the vertical magnetic field in the undulator (full line). The dotted line is a fit with the function $\frac{5.096}{1+\left(\frac{s}{289.01}\right)^8}\sin\left(-\frac{s}{45.42}\right)$ of the longitudinal coordinate s.

mum distortion $x(s)$ at position s, calculated for the four dipole model in appendix I, is given by :

$$\hat{x}(s) = \frac{\theta l}{2\sin\pi Q}\sqrt{\frac{\beta(s)}{\beta}}$$

where θ is the kick angle associated with a single dipole, the unlabeled β being an average over the undulator, i.e. about 105m. With the LHC fractional part of the tune of 0.28 and for a maximum value of the β-function in the arcs of 200m, the maximum value of $x(s)$ in the arcs is 0.052mm. The calculation with MAD for the same model gives the same number.

It is possible to cancel the closed orbit distortion in the arcs, by localizing the closed orbit distortion in the undulator region by means of a local closed orbit bump. This is shown in Figure 5. The horizontal closed orbit correctors used are close to Q5 on the left, Q6 and Q8 on the right. The respective kick angles are 0.1, -0.007 and -0.005μrad, i.e. smaller than 0.2% of the nominal strength.

The actual undulator might have a non-zero integrated field. We express the associated kick as a fraction η of the kick of a single dipole in the four dipole model. The associated maximum closed orbit distortion $\hat{x_e}(s)$ is given by :

$$\hat{x_e}(s) = \frac{\eta\theta}{2\sin\pi Q}\sqrt{\beta(s)\beta} = \hat{x}(s)\frac{\eta\beta}{l}$$

We have seen that the maximum value of $\hat{x}(s)$ is small and that the corrector strength to cancel it is very small. Therefore a value of $\hat{x_e}(s)$ of the same order as $\hat{x}(s)$ is
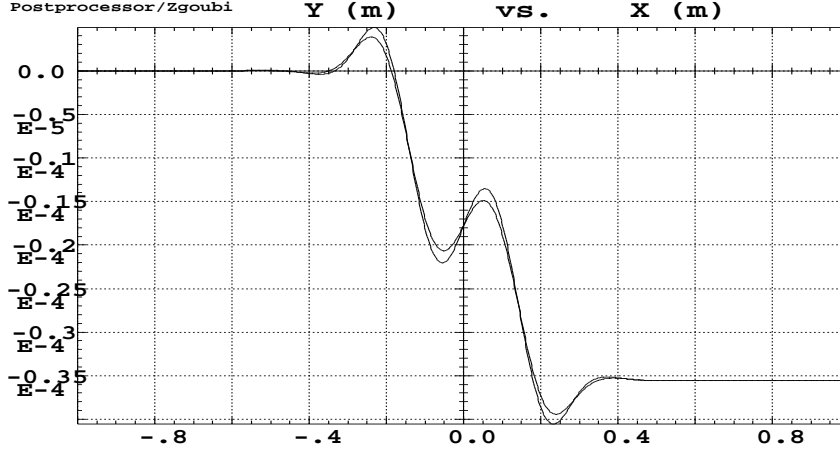
3

Y (m)   **vs.**   **X (m)**

Figure 4: Trajectory of a 450GeV proton starting on the undulator axis obtained by ray tracing. The curve with the larger amplitude of the oscillations corresponds to a starting point with a vertical offset of 3cm.

acceptable, i.e. an error of the integrated field of the undulator of the order of $Bl^2/\beta = 9 \cdot 10^{-4}$Tm, i.e. 9Gauss.m is quite acceptable. An error 10 times as large would take less than 2% of the maximum corrector strength, i.e. it is also acceptable. An error 100 times as large is not acceptable as it consumes too much of the corrector strength and reduces the aperture by 2mm at a critical point, opening a risk of systematic quench of D3.

4 Quadrupole effects.

If a particle trajectory passes with a non-zero angle θ, through a place where the vertical magnetic field changes abruptly, this produces a focusing effect in the vertical plane, as well as non-linear components. The focusing strength is given by $2\theta B/(\mathcal{B}\rho)$, where $(\mathcal{B}\rho)$ is the magnetic rigidity of the particles. We can evaluate an order of magnitude of the effect by considering a trajectory which enters the undulator perpendicular to the first dipole. In this case there are two places where the trajectory crosses dipole edges with opposite field changes and opposite angles. The associated vertical tune-shift ΔQ_y is given by :

$$\Delta Q_y = \frac{\beta\theta}{\pi}\frac{B}{(\mathcal{B}\rho)}.$$

Its numerical value is 0.0001. The calculation done with both MAD and ray tracing (see section 5) give smaller results as the actual angles are not those quoted above. In any case the tune-shift due to the undulator is totally negligible, as well as the associated β-beating.
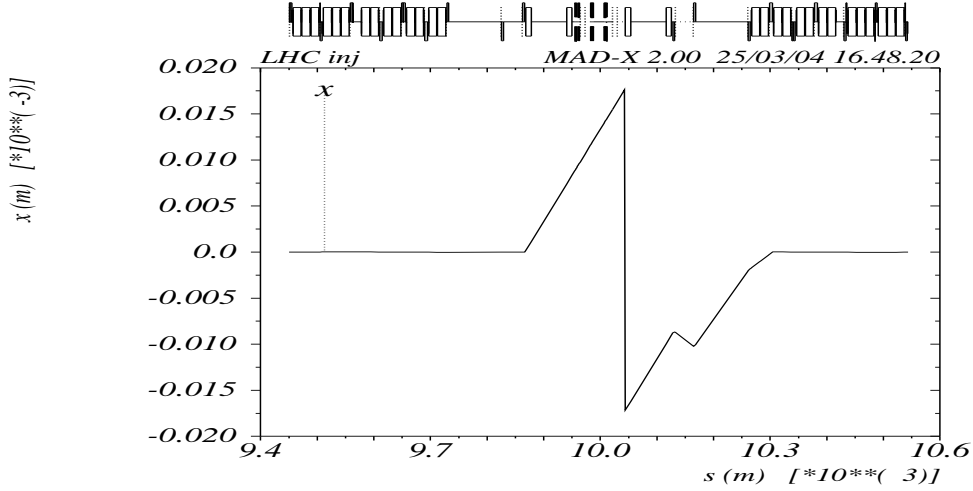
4

Figure 5: localization of the closed orbit distortion due to the undulator by means of three closed orbit correctors (strength smaller than 0.1μrad). The displacement of the trajectory due to the undulator is clearly seen on the figure center.

The quadrupole effect has been analyzed by means of ray tracing. The integration of trajectories has been done over the whole LHC. Only chromaticity sextupoles have been included in order to compare the multipole effects due to the 3D field of the undulator with those of these sextupoles. A comparison between the various computations is given in table 1.

Table 1: Optical parameters in LHC, with or without fringe fields (FF), undulator. The anharmomicities are evaluated from tracking with a 13σ amplitude.

	No FF, undulator off		FF + undulator off	FF+undulator on
	MAD	**ray-tracing**		
Frac. Q_x / Q_y	0.2800 / 0.3100	0.2800 / 0.3100	0.2798 / 0.3098	0.2798 / 0.3098
Q'_x / Q'_y	1.978 / 1.751	1.951 / 1.812	1.952 / 1.816	1.953 / 1.816
Q''_x / Q''_y		157 / 78	137 / -8	137 / 10
$\frac{\pi\Delta Q_x}{\Delta\epsilon_x}$ / $\frac{\pi\Delta Q_x}{\Delta\epsilon_y}$ / $\frac{\pi\Delta Q_y}{\Delta\epsilon_y}$		$-$ / -1540 / 512	423 / -1670 / 590	470 / -1630 / 630

5   Intrinsic multipole effects.

As the field of the undulator is essentially three dimensional, the description of the multipole errors used for the usual magnets of circular machines is not relevant a priori. Actually it can be shown that the usual description is nevertheless valid for the integrated transverse field components (see appendix II). Tolerances for these components are established in section 6.

5

The multipole effects associated with the longitudinal variation of the vertical magnetic field are addressed in appendix III. It is shown that the non-linearities are expected to have an effect only in the vertical plane.

From trajectory tracking a little above the LHC dynamic aperture at injection, i.e. at 13σ, the three anharmonicities have been evaluated. They are listed in table 1.

Trajectories starting with a radial amplitude of 30σ in both planes have been tracked over $5\,10^4$ turns using ray tracing. The phase space plots associated with the machine and its chromaticity sextupoles are shown on figure 6. The same plots obtained by adding the undulator are shown on figure 7. The difference between the plots is
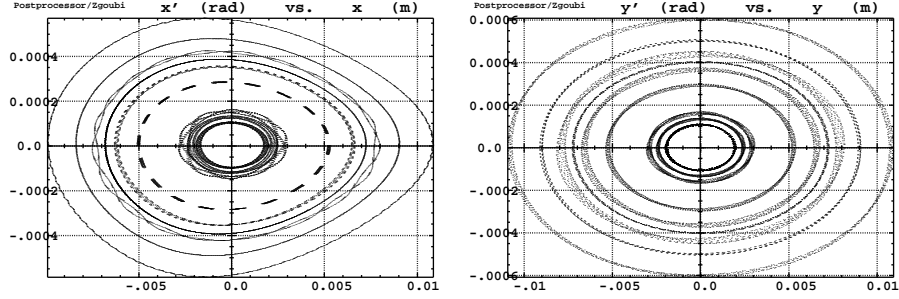
Figure 6: Initial amplitudes of 20, 25 and 30σ, three initial angles $15°$ $45°$ and $75°$ in the {x,y} plane, $5\,10^4$ turns. Fringe fields set in all dipoles and quadrupoles, chromaticity sextupoles on, no undulator.

Figure 7: Initial amplitudes of 20, 25 and 30σ, , three initial angles $15°$ $45°$ and $75°$ in the {x,y} plane, $5\,10^4$ turns. Fringe fields set in all dipoles and quadrupoles, chromaticity sextupoles on, undulator excited at full field.
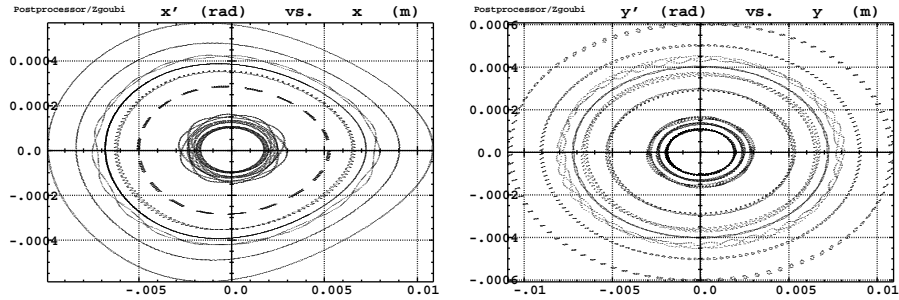
indistinguishable with the exception of two trajectories with slightly different tunes in the vertical plane. The detunings obtained at 30σ are very close to each other, they are listed in table 2. This shows that the intrinsic non-linearities due to the undulator are very small compared with those associated with the chromaticity sextupoles. As the latter are negligible, the intrinsic non-linearities associated with the undulator are even more negligible.

As the non-linearities are negligible and as dispersion is zero at the location of the

undulator, no effect on the non-linear chromaticity is expected. This has been checked by ray tracing and Fourier analysis as for the case of large betatron amplitudes. The differences in tunes for a relative momentum deviation of ± 0.003 is in the range of some 10^{-5} which is totally negligible.

	Angle (deg.)		
N_σ	15°	45°	75°
0	0.279815 / 0.309758	0.279815 / 0.309759	0.279815 / 0.309759
1	0.279795 / 0.309720	0.279789 / 0.309726	0.279784 / 0.309734
5	0.279848 / 0.309489	0.279708 / 0.309648	0.279505 / 0.309829
9	0.280047 / 0.308760	0.279386 / 0.309438	0.278794 / 0.310071
13	0.280239 / 0.3077438	0.278961 / 0.309086	0.277731 / 0.310363
20	0.280744 / 0.305190	0.27779 / 0.308167	0.274812 / 0.311183
25	0.281192 / 0.302753	0.27658 / 0.307286	0.271918 / 0.312057
30	0.281651 / 0.299863	0.27498 / 0.306312	0.268394 / 0.313069
	15°	45°	75°
0	0.279796 / 0.309783	0.279796 / 0.309783	0.279796 / 0.309783
1	0.279798 / 0.309767	0.279792 / 0.309775	0.279787 / 0.309784
5	0.279853 / 0.309537	0.279711 / 0.309683	0.279513 / 0.309914
9	0.280056 / 0.308807	0.279392 / 0.309498	0.278798 / 0.310108
13	0.280244 / 0.307781	0.278971 / 0.309120	0.277735 / 0.310444
20	0.280749 / 0.305218	0.277794 / 0.308199	0.274818 / 0.311232
25	0.281198 / 0.302779	0.276596 / 0.307332	0.271924 / 0.312097
30	0.281658 / 0.299890	0.274994 / 0.306361	0.268404 / 0.313113

Table 2: Tunes Q_x/Q_y vs $N\sigma$ and angle. (Fourier expansion, 1000 turns). Upper table : machine as for fig. 6, lower table : machine as for fig. 7

6 Multipole effects due to imperfections

Because of mechanical imperfections the integrated field of the undulator may not be zero. In particular the integral may vary with the distance to the axis. This integral can be described with a polynomial of the horizontal position. Because of the small variation of the phase advance in the undulator and as the intrinsic non-linearities have been shown to be negligible, it is legitimate to identify this polynomial with that of a standard description of dipole errors in LHC. This is shown in appendix II.

If the associated multipole components have the same values as the random multipole components in a single main dipole, they will have no measurable effect on the dynamic aperture. The integrated components are given as a function of the dipole field errors b_n by the formula :

$$l \; \partial^{n-1} B / \partial x^{n-1} = \frac{(n-1)! \; b_n \; l_{dip}}{\rho R^{n-1}} (\mathcal{B}\rho) = 7.7 \, 10^{-4} \frac{(n-1)!}{0.017^{n-1}} b_n,$$

7

where R is the reference radius (0.017m) and ρ the radius of curvature in the dipoles. The numerical formula gives the integrated components in Tm^{2-n}, b_n being given in units of 10^{-4}. The values of the integrated components are given in Table 3. As they are associated with the r.m.s. dipole field errors, errors larger by a factor of 3 are acceptable.

It is worth comparing these values to reference values at injection, like the sextupole component of the chromaticity sextupoles of $45Tm^{-1}$ or the octupole component in the Landau octupoles of $60000Tm^{-2}$.

n	3	4	5	6	7	8	9	10
$b_{n,d}$	1.47	0.51	0.43	0.09	0.22	0.04	0.07	0.01
$l\,\frac{\partial^{n-1}B_y}{\partial x^{n-1}}/Tm^{-n+2}$	7.8	480	$5.4\ 10^4$	$5.8\ 10^6$	$5\ 10^9$	$3.8\ 10^{11}$	$3.1\ 10^{14}$	$2.4\ 10^{16}$
$a_{n,d}$	0.48	0.51	0.34	0.17	0.08	0.08	0.12	0.01
$l\,\frac{\partial^{n-1}B_x}{\partial x^{n-1}}/Tm^{-n+2}$	2.5	480	$4.3\ 10^4$	$8.9\ 10^6$	$1.8\ 10^9$	$7.6\ 10^{11}$	$5.3\ 10^{14}$	$2.4\ 10^{16}$

Table 3: Possible multipole errors in the undulator at a radius of 17 mm. The measurement is done with a rotating coil extending over the whole magnet. **Errors larger by a factor three, i.e. equal to the maximum error set in tracking, are acceptable.**

7 Conclusion

The introduction of the undulator to measure the LHC beam size does not have any consequence from the point of view of single particle effects. The closed orbit distortion has a maximum amplitude smaller than 0.04mm. It can be easily corrected with the closed orbit correctors. The tune shifts are completely negligible. The intrinsic non-linearities are probably negligible because the phase advance across the undulator is small. The field errors computed from a polynomial fit of the variation of the vertical field along the x axis should be smaller than those given in Table 3 above in order to have no effect on the dynamic aperture. The integrated field could differ from zero by 90Gauss.m at most.

References

[1] R. Jung and H. Schmickler, CERN workshop on emittance measurement (July 2000).

[2] F. Méot, L. Ponce, J. Bosser, R. Jung, DIAGNOSTIC WITH SYNCHROTRON RADIATION OF THE LHC PROTON BEAMS, Proceedings of EPAC2002, Paris, France.

[3] Y. K. Wu, J. Li, S. F. Mikhailov, V. Litvinenko, Nonlinear Dynamics in the Duke Storage Ring with FEL Wigglers, PAC2003 (May 2003).

[4] F. Méot and S. Valéro, Zgoubi user's guide, Report CEA/DSM/DAPNIA/SEA-97-13, Saclay, October 1997.

[5] C. Vollinger, private communication (June 2003, LHC days).

Appendix I

Closed orbit distortion due to two close opposite dipoles

The centers of the two dipoles are labeled 1 and 2. The closed orbit distortion $x(s)$ at the position s in the machine, associated with a deflection θ in dipole 1 and $-\theta$ in dipole 2 is given by :

$$x(s) = \frac{\theta\sqrt{\beta(s)}}{2\sin\pi Q} \left[\sqrt{\beta_1}\cos(\psi(s)+\mu_1) - \sqrt{\beta_2}\cos(\psi(s)+\mu_2) \right]$$

This expression can be expanded in terms of $\cos(\psi(s)+\mu_1)$ and $\sin(\psi(s)+\mu_1)$. From the coefficients of these two members, the maximum amplitude $\hat{x}(s)$ of the distortion in the machine is :

$$\hat{x}(s) = \frac{\theta\sqrt{\beta(s)}}{2\sin\pi Q} \sqrt{\beta_1 + \beta_2 - 2\sqrt{\beta_1\beta_2}\cos(\mu_2 - \mu_1)}$$

For the case where the length of the dipoles (0.14m in our case) is very small compared with β_1 and β_2 (105m in our case), the phase advance can be approximated with $l/\sqrt{\beta_1\beta_2}$ and $\beta_2 \simeq \beta_1 - 2\alpha_1 l$. Introducing these expressions in the above equation, we obtain eventually :

$$\hat{x}(s) = \frac{\theta l}{2\sin\pi Q} \sqrt{\frac{\beta(s)}{\beta_1}} \left(1 + \frac{\alpha_1 l}{\beta_1}\right)$$

As α_1=0.11 in our case, $\hat{x}(s)$ is very well approximated with :

$$\hat{x}(s) = \hat{x}(s) = \frac{\theta l}{2\sin\pi Q} \sqrt{\frac{\beta(s)}{\beta_1}}$$

For a value of $\beta(s)$ of 200m and a field of 2.5T in the dipoles, the value of $\hat{x}(s)$ is 0.027mm at 450GeV.

For our case, there are two sets of two opposite dipoles which have an additive effect if the phase advance between both is neglected, so the eventual maximum distortion in the arcs will be 0.054mm.

Appendix II

2D Maxwell equations

We consider an isolated magnet of finite length and the Maxwell equations in free space to compute the magnetic field around its axis (there is no current). The magnet axis is the s axis and the transverse axis are x and y, like in a circular machine.

The Maxwell equations in free space reduce to :

$$\frac{\partial B_x}{\partial x} + \frac{\partial B_y}{\partial y} + \frac{\partial B_s}{\partial s} = 0 \tag{1}$$

$$\frac{\partial B_x}{\partial y} = \frac{\partial B_y}{\partial x}, \quad \frac{\partial B_x}{\partial s} = \frac{\partial B_s}{\partial x}, \quad \frac{\partial B_y}{\partial s} = \frac{\partial B_s}{\partial y} \tag{2}$$

We use the property that integration and derivation can be swapped. Integrating equation 1 with respect to s, we obtain :

$$\frac{\partial}{\partial x} \int_{-\infty}^{+\infty} B_x ds + \frac{\partial}{\partial y} \int_{-\infty}^{+\infty} B_y ds + [B_s]_{-\infty}^{+\infty} = 0 \tag{3}$$

As there is no magnetic field far outside the magnet, $[B_s]_{-\infty}^{+\infty} = 0$ and equation 1 reduces to a 2D equation for the transverse fields integrated over the longitudinal axis.

Then integrating the first equation in 2 provides the "second Maxwell equation for 2D fields".

Integrating the next two equations expresses that B_s is constant since both B_x and B_y are zero far outside the magnet. As the total magnetic field is zero far outside the magnet, the integral of B_s is also zero.

Eventually what remains are two 2D equations for the integrated B_x and B_y.

Appendix III

Dipole end field

We consider the 2D problem of the magnetic field of a dipole in the hard edge approximation. The longitudinal s axis is perpendicular to the magnet end and there is no variation with the horizontal coordinate x (we assume an extension in x much larger than the gap). We assume that the field of normalized value $1/\rho$ is vertical inside the dipole (no x variation), i.e. : $b_y = \frac{f(s)}{\rho}$. $f(s)$ is a dimensionless function of the longitudinal variable s which has a zero integral over the undulator by definition. This magnetic field satisfies the first Maxwell equation (see appendix II) but not the second one (2D). Inserting this expression in the second equation, we obtain :

$$\frac{\partial b_s}{\partial y} = \frac{\partial b_y}{\partial s} = \frac{f'(s)}{\rho}$$

where $f'(s)$ is the derivative of $f(s)$ with respect to s. Integrating this equation, we obtain $b_s(s) = \frac{yf'(s)}{\rho}$ since there is no field outside the dipole and no x variation. Then putting this expression into the first equation, we obtain the next term of the expansion of B_y with respect of y. This procedure can be iterated. We obtain eventually :

$$b_y = \frac{1}{\rho}\left[f(s) - f''(s)\frac{y^2}{2!} + f^{(4)}(s)\frac{y^4}{4!} + ...\right]$$

$$b_s = \frac{1}{\rho}\left[f'(s)y - f^{(3)}(s)\frac{y^3}{3!} + f^{(5)}\frac{y^5}{5!} + ...\right],$$

where $f^{(n)}(s)$ is the nth derivative of the function $f(s)$. It is easy to check that these expressions fulfill the 2D Maxwell equations.

The non-linear kick can be calculated exactly in a **fixed frame** by integrations of the equation of motion :

$$x'' = y'b_s - b_y \ , \ y'' = x'b_s(b_x = 0).$$

The integration of x'' can be performed exactly except for the first term. Taking the origin at the undulator center and d being its half length, i.e. the distance at which the field vanishes, we obtain :

$$x'(s) = x'(-d) + \frac{1}{\rho}\left[-\int_{-d}^{s} f(t)dt + \frac{y^2}{2!}f^{(1)}(s) - \frac{y^4}{4!}f^{(3)}(s) + \frac{y^6}{6!}f^{(5)}(s) - .....\right]$$

as $f(-d)$ and $f^{(n)}(-d)$ are all zero.

The total kick can be obtained by setting $s = d$. As $\int_{-d}^{+d} f(t)dt$, $f(+d)$ and $f^{(n)}(+d)$ are also zero, there is no kick in the horizontal plane due to the non-linear fields associated with the longitudinal variation of the vertical field. This does not mean

that there is no effect. Indeed we have seen that there is a displacement due to the non-zero value of $\int_{-d}^{+d} du \int_{-d}^{u} f(t)dt$. Assuming that the variation of y is small along the undulator, the above equation can be further integrated. It gives :

$$x(s) = x(-d) + x'(-d)s + \frac{1}{\rho}\left[-\int_{-d}^{s} du \int_{-d}^{u} f(t)dt + \frac{y^2}{2!}\int_{-d}^{s} f(t)dt - \frac{y^4}{4!}f'(s) + \frac{y^6}{6!}f^{(3)}(s) - .....\right]$$

Again due to the absence of field outside of the undulator, the total displacement is only due to the first term. Thus, within the approximation that y does not vary along the undulator, there is no non-linear effect in the horizontal plane. In the moving frame used to describe the betatron oscillations there are kinematical non-lirear terms in the equation of motion. Thus only these terms, which are usually neglected in the analysis of betetron oscillations contribute to the non-linearity of the undulator in the horizontal plane.

In the vertical plane, the integration of the equation of motion cannot be done simply as we cannot assume that the coordinate x does not vary much along the undulator.

The assumption that the y coordinate varies little is associated with the small phase advance over the length of the undulator. The optics functions calculated in the undulator are given in Table 4.

	β_x/m	$\mu_x/2\pi$	D_x/m	β_y/m	$\mu_y/2\pi$
entrance	105.80	24.29212899	-0.000138	246.15	22.3715008
mid first pole	105.72	24.29247783	0.0005025	246.51	22.37166539
mid second pole	105.76	24.29236971	-0.000141	246.39	22.3716042
mid third pole	105.70	24.29279118	-0.000124	246.81	22.37178491
end undulator	105.63	24.29328824	-0.000105	247.31	22.37199749

Table 4: Optics functions inside the undulator computed with MADX. The poles are modeled with a sequence of constant field dipoles of length 0.02m as described in section 2.